Hindawi
International Journal of Energy Research
Volume 2024, Article ID 9717587, 16 pages
https://doi.org/10.1155/2024/9717587

Research Article

Effect of Elevated Temperature and Internal Pressure due to Severe Accidents on the Internal Pressure Capacity of Prestressed Concrete Containment Vessel

Sangwoo Lee,[1] **Woo-Min Cho**,[2] **Hoyoung Son**,[1] **Han-Sang Woo**,[2] **Bu-Seog Ju**,[1] **and Yoon-Suk Chang**[2]

[1]*Department of Civil Engineering, Kyung Hee University, Yongin-si, Gyeonggi-do, Republic of Korea 17104*
[2]*Department of Nuclear Engineering, Kyung Hee University, Yongin-si, Gyeonggi-do, Republic of Korea 17104*

Correspondence should be addressed to Bu-Seog Ju; bju2@khu.ac.kr and Yoon-Suk Chang; yschang@khu.ac.kr

Received 30 October 2023; Revised 18 December 2023; Accepted 20 December 2023; Published 24 January 2024

Academic Editor: Paolo Castaldo

The integrity of containment buildings in nuclear power plants is crucial for preventing the release of radioactive materials during severe accidents. This study investigates the effect of the uncertainty in temperature-dependent strength of concrete on the internal pressure capacity of prestressed concrete containment vessel (PCCV). To this end, a high-fidelity finite element model is developed and the uncertainty in concrete material properties due to temperature variations is taken into account for a finite element analysis with internal pressure and temperature histories. In addition, two limit states of PCCV, such as onset of leakage and functional failure, are defined to investigate internal pressure capacity depending on the different damages to PCCV. The results provide insights into the behavior of PCCV under severe accident conditions and the impact of the uncertainty in the concrete material due to temperature on their performance, in terms of the leakage of PCCV. This research enhances the understanding of PCCV's response to internal pressure and temperature and contributes to the safety assessment of nuclear power plants.

1. Introduction

Nuclear power plants rely on multiple barriers to prevent the release of radioactive materials and safeguard public health and the environment [1]. Among these barriers, the containment building plays a crucial role in enclosing and protecting critical equipment, such as reactors, steam generators, and safety systems, ensuring the safe operation of nuclear power plants. However, during severe accident scenarios characterized by increased internal pressure and temperature, the primary barriers may fail, leaving the containment building as the last line of defense against the leakage of radioactive fission products into the environment [2]. Consequently, ensuring the integrity of containment buildings during beyond-design accidents has become a matter of great concern in the nuclear industry, leading to various experiments investigating their structural behavior under internal pressure [3–6].

The Nuclear Power Engineering Corporation (NUPEC) and the Nuclear Regulatory Commission (NRC) cosponsored and funded a research project at Sandia National Laboratories (SNL) to study the ultimate pressure capacity (UPC) of prestressed concrete containment vessels (PCCV). As part of this project, a 1 : 4-scale PCCV, representative of existing PCCVs for pressurized water reactors (PWR) in Japan, underwent a UPC test [7]. This test served as the foundation for the International Standard Problem 48 (ISP48), proposed during the June 2002 meeting of the Committee on the Safety of Nuclear Installations (CSNI) [8]. The objectives of ISP48 were twofold: firstly, to enhance the understanding of the internal pressure capacities of containment buildings by incorporating the results of the 1 : 4-scale PCCV test results and finite element analysis and, secondly, to investigate the effects of increased internal pressure and temperature resulting from severe accident events on containment buildings.

Since conducting actual experiments on PCCVs subjected to combined internal pressure and temperature loads has limitations, numerous studies have employed finite element models to investigate and estimate their behavior [8–14]. Therefore, it is crucial to develop a high-fidelity finite element (FE) model that considers the degradation of material properties as temperature increases. Many empirical studies have already examined the degradation of concrete and steel strength with temperature variations, as well as the reduction of elastic modulus. These studies have quantified the extent of degradation through experimental data. However, previous temperature-related studies, including ISP48, typically analyzed FE models by incorporating deterministic degradation of material properties with temperature, disregarding the uncertainty in material property resulting from temperature changes. Notably, concrete exhibits significant uncertainty in its material properties under varying temperatures [8, 15, 16]. Consequently, it is necessary to investigate the internal pressure capacity of PCCVs while considering the uncertainty in concrete material properties due to temperature changes.

Furthermore, most temperature-related containment studies face limitations in terms of generalizing the effect of temperature on PCCVs, as they often focus on analyzing a single temperature and pressure scenario. Additionally, while many studies have examined the yield or failure of individual components such as rebars, tendons, liners, and concrete under temperature and internal pressure changes, the internal pressure capacity of PCCVs has not been evaluated in terms of the crucial factor of leakage during severe accidents at nuclear power plants.

This study is aimed at investigating the effect of the uncertainty in concrete material combined with various temperature changes on the internal pressure capacity of PCCVs, with a specific focus on leakage as a global response instead of the damage to each component. To accomplish this, two limit states, namely, the onset of leakage and functional failure, are defined based on experimental data. The study evaluates the effect of temperature changes on the internal capacity of PCCVs and identifies the impact of uncertainty in concrete material properties resulting from temperature changes. The uncertainties in concrete material properties considering temperature variations are defined as upper and lower bound levels, utilizing data provided by Hessheimer and Mathet [8]. The study examines the change in internal pressure capacity according to the uncertainty in concrete material properties, employing the defined upper and lower bound material properties. Two temperature and internal pressure scenarios from ISP48 [8] are utilized for analysis: saturated steam condition (SSC) and station blackout (SBO). The SSC scenario exhibits a relatively smooth temperature change up to 200°C, suggesting no reduction in steel strength, but a slight reduction in concrete properties is anticipated considering the uncertainty in concrete properties. Moreover, SSC scenarios assuming internal temperature increases to 400°C and 600°C are analyzed to examine the effect of various temperatures on containment buildings and to generalize the impact of temperature on PCCVs. The SBO represents a severe accident scenario characterized by rapid temperature changes up to 600°C due to hydrogen burn, allowing examination of the effects of temperature and material uncertainty on PCCVs.

2. Experiment of Prestressed Concrete Containment Vessel

The 1 : 4-scale PCCV test conducted by SNL is aimed at evaluating the structural response and failure modes of a scaled-down model of the PCCV when subjected to overpressurization. This test provided valuable insights into the behavior of the containment vessel under extreme conditions and assessed its structural integrity.

The test model consisted of a cylindrical reinforced concrete wall with a hemispherical dome and basemat, to which a continuous steel liner plate was attached. Prestressing tendons were utilized in both vertical and horizontal directions, anchored to the tendon gallery of the concrete basemat and buttresses at 90 and 270 degrees, respectively, to apply balanced prestressing forces to the containment vessel. This approach is aimed at preventing local concentrations of deformation or damage [7].

The constructed test model was subjected to a pressurization plan designed to define the failure modes with a designated design pressure (P_d) of 0.39 MPa, fulfilling the experimental objectives. During the test, an elastic response was observed up to 1.3 to 1.5 P_d, despite the prestress being overcome at 1.2 P_d and the initiation of concrete tensile cracking occurring at 1.13 P_d. Beyond 1.5 to 2.5 P_d, the tensile stiffness of the concrete was significantly reduced due to major cracks, maintaining its linear response against pressurization. The onset of liner tearing and leakage was observed in the vicinity of the equipment hatch (EH) between 2.4 and 2.5 P_d, accompanied by increased nonlinearity, specifically in the midsection of the cylindrical wall, attributed to the generalized yielding in the hoop direction.

To achieve the objectives of investigating the inelastic response of the structure, the scaled PCCV was kept pressurized as part of limit state test (LST) until a pressure of 3.3 P_d was reached, at which the leak rate exceeded the capacity of the pressurization system using nitrogen gas. Post-test examination for the functional failure revealed an approximate global hoop strain of 0.4% for the structure, along with the formation of 26 tears in the interior steel liner. Subsequently, the structural failure mode test (SFMT) was conducted by repressurizing the model using water to observe the inelastic response until the pressure could no longer be retained or structural failure occurred. Finally, at an effective peak pressure of 3.63 P_d, the expanded PCCV started to rupture near the midheight of the concrete wall at an azimuth of 6 degrees.

3. Finite Element Model of a 1 : 4-Scale PCCV

3.1. Development of the Finite Element Model for a 1 : 4-Scale PCCV. The 1 : 4-scale PCCV FE model was developed [17], and the concrete damage plasticity (CDP) model was used

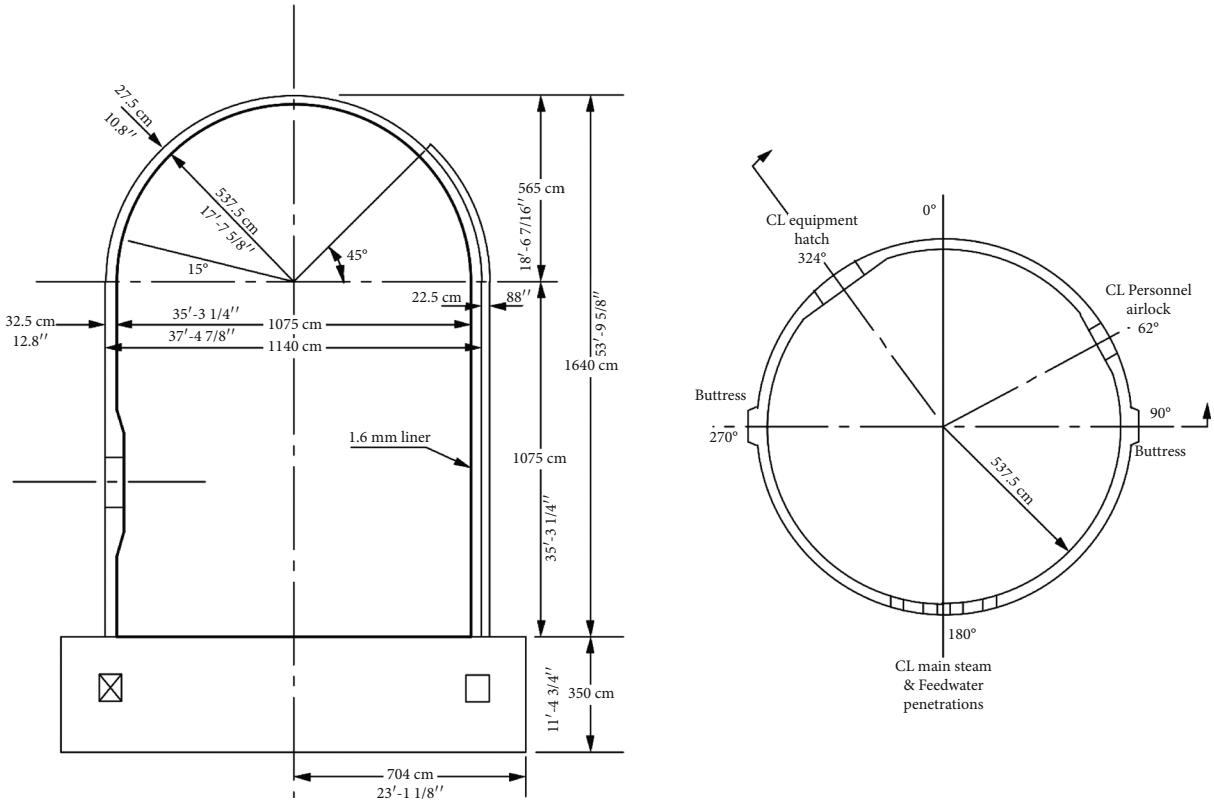

Figure 1: Descriptions of 1 : 4-scale PCCV [7, 17].

for predicting nonlinear response of PCCV [18, 19]. The concrete structure consists of a cylinder wall with an inner radius of 5,375 mm, a thickness of 32.5 mm, and a height of 10.75 m. The hemispherical dome has the same radius and thickness as the cylinder, and basemat has a radius of 7,040 mm and a height of 3,500m. Buttresses are attached to the cylindrical wall at azimuths of 90 and 270 degrees. Major discontinuities, such as equipment hatch (EH) with a 770 mm radius hole and airlock (AL) with a 330.5 mm radius hole, were considered. However, minor discontinuities, such as main steam (MS) and feed water (FW), were excluded based on previous research indicating their minimal effect on the global behavior of the structure. The configuration of the 1 : 4-scale PCCV is illustrated in Figure 1.

The concrete structure was meshed globally using solid elements of the continuum, 3D, 8-node, reduced (C3D8R), with a mesh size of 400 mm and 4 elements in the thickness direction. The 1.6 mm steel liner attached inside the concrete wall was simulated using membrane elements, 3D, 4-node (M3D4), with the same mesh size as the concrete structure. The rebars and tendons embedded in the concrete were connected programmatically using the embedded element option. Truss elements, 3D, 2-node (T3D2), with a global mesh size of 0.3 m, were employed for the rebars and tendons.

The bottom surface of basemat was fully constrained, including displacement and rotation in all directions. The dead weight of the structure was considered, and prestressing forces were applied to the tendon system using predefined stress option. The internal pressure was applied to the inner surface of the steel liner plate in different ways for validation, specifically for saturated steam conditions (SSC) and station blackout (SBO). Detailed explanations of the applied pressures are provided in the corresponding sections.

3.2. Validation of the Finite Element Model: Comparison with Test Results. To determine the optimum mesh size for the 1 : 4-scale PCCV FE model, a mesh convergence study was conducted to ensure the accuracy and the efficiency of the numerical analysis. The same internal pressure up to 1.29 MPa, corresponding to the limit state test (LST), was applied, and the peak radial displacements at the free-field azimuth of 135 degrees and a height of 6,200mm were compared for different numbers of elements in each analysis (Figure 2). The results indicated that the expansion due to the refined mesh converged with a mesh density of approximately 120,000 elements, using a global mesh size of 400 mm. Thus, this mesh shape was chosen for the FE model during the overpressurization analysis as shown in Figure 2.

Furthermore, validation was conducted using the converged containment vessel model by comparing the test and analysis results as shown in Figure 3. Specifically, azimuths of 135 (free field) and 324 (centerline of EH) degrees and the heights of 4,680 mm and 6,200mm were considered. The radial displacements with increasing internal pressure showed

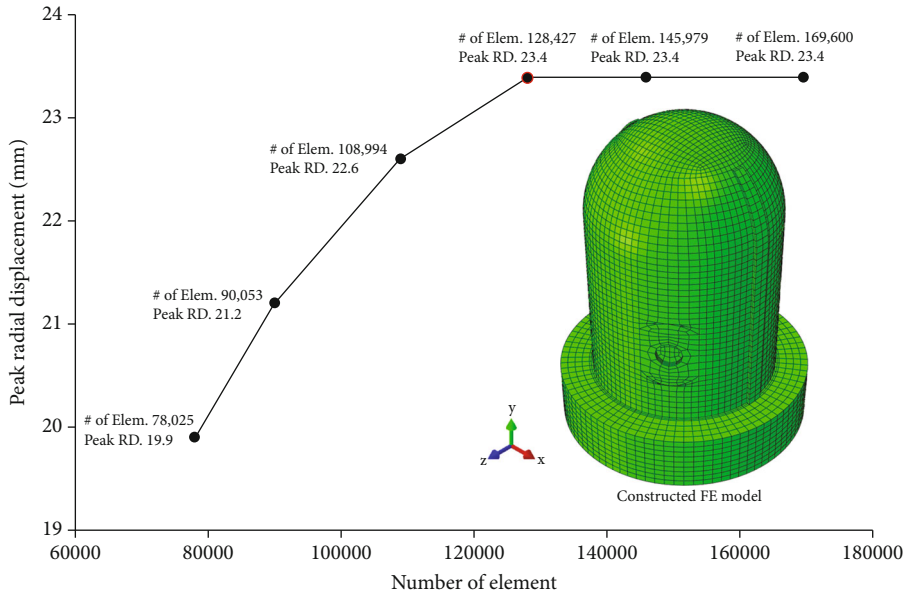

Figure 2: Mesh density analysis.

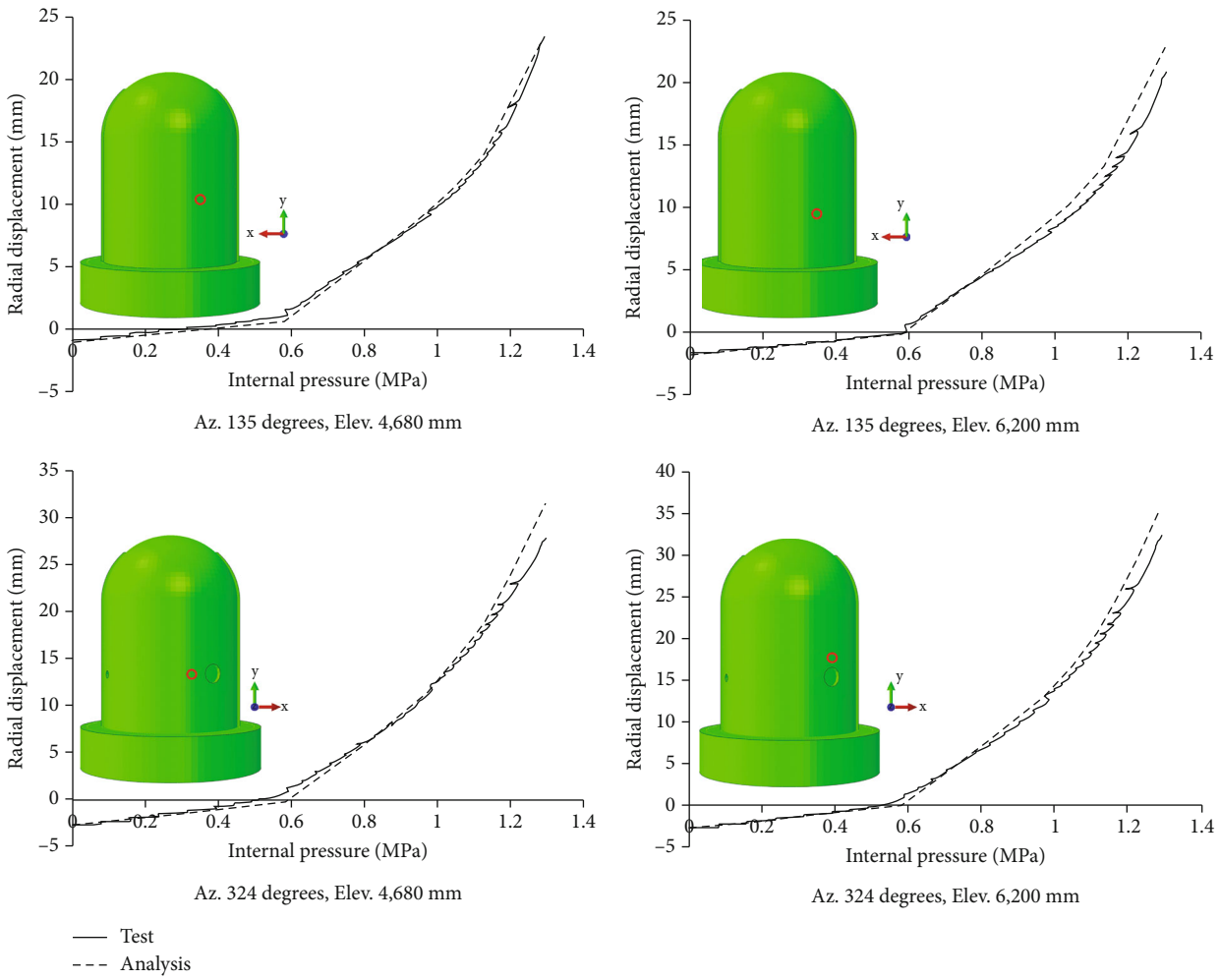

Figure 3: FE model validation through radial displacement comparison.

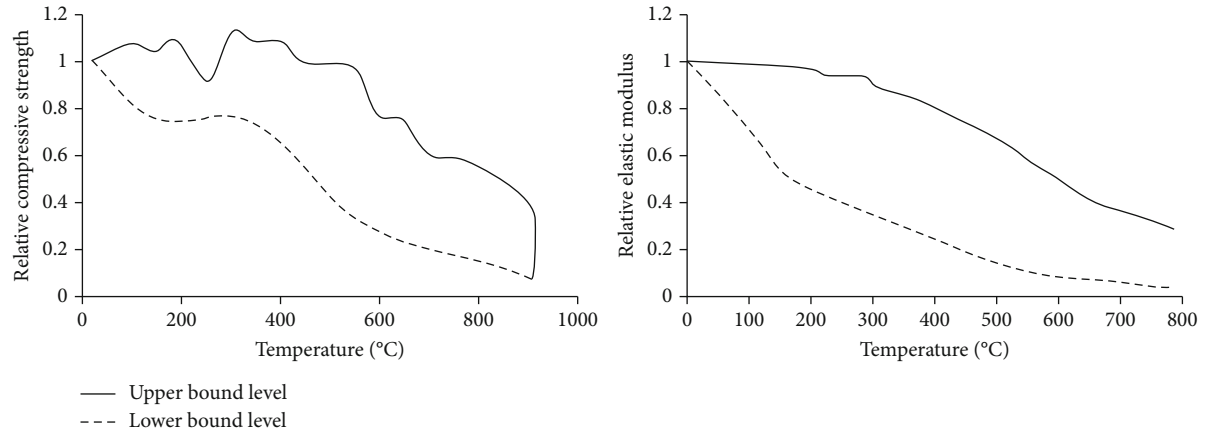

(a) Kodur 2014 [16]

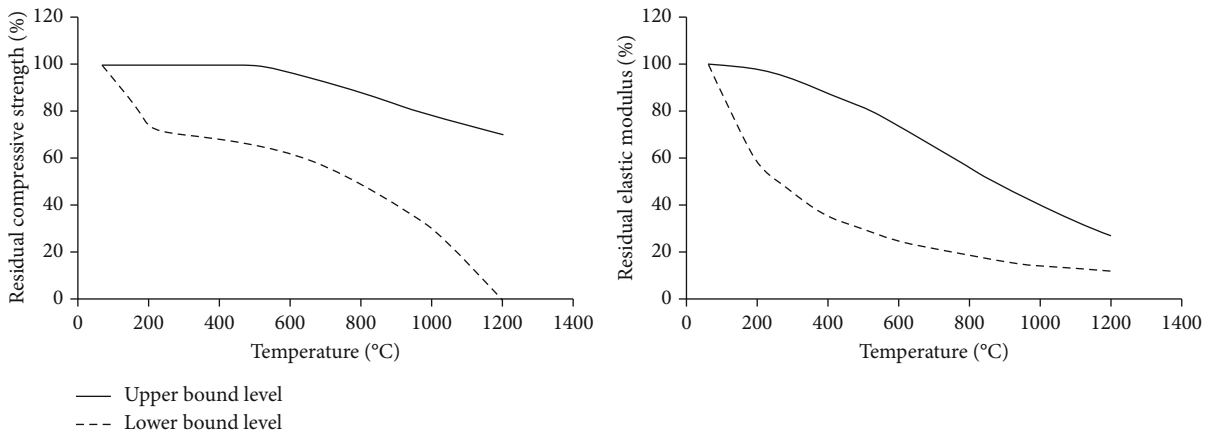

(b) Hessheimer and Mathet 2005 [8]

Figure 4: Variation in compressive strength and elastic modulus of concrete as a function of temperature.

that the developed FE model provided comparable results in terms of peak displacements and the onset of nonlinearity after 0.6 MPa, attributed to the yielding of the structure, when compared to the test results (Figure 3). Through the mesh convergence study and validation process, it was verified that the developed FE method accurately and efficiently simulates the behavior of the 1 : 4-scale PCCV under internal pressure.

3.3. Uncertainty Analysis of Concrete Material Properties with Temperature Variation. Numerous studies have investigated the effects of temperature change on the material properties of concrete, revealing that properties such as compressive strength, Young's modulus, and tensile strength degrade as the temperature increases [15, 16, 20–33]. Equations developed based on these studies [28–33] are commonly used to analyze the behavior of concrete structures subjected to temperature variations. However, there exist significant discrepancies in the values of concrete material properties obtained from equations. In addition, some studies have provided a range of possible material properties according to temperature, as depicted in Figure 4 [8, 15, 16].

Table 1: Residual concrete compressive strength according to temperature (%).

	100°C	200°C	300°C	400°C	500°C	600°C
Upper bound level	100	100	100	100	100	97
Lower bound level	95	75	70	68	66	62

Table 2: Residual concrete elastic modulus according to temperature (%).

	100°C	200°C	300°C	400°C	500°C	600°C
Upper bound level	100	100	100	100	100	98
Lower bound level	97.5	86.6	84.9	82.4	81.2	78.8

Table 3: Residual concrete tensile strength according to temperature (%).

	100°C	200°C	300°C	400°C	500°C	600°C
Upper bound level	100	100	100	100	100	98
Lower bound level	95.0	75.0	70.4	68.0	66.0	62.0

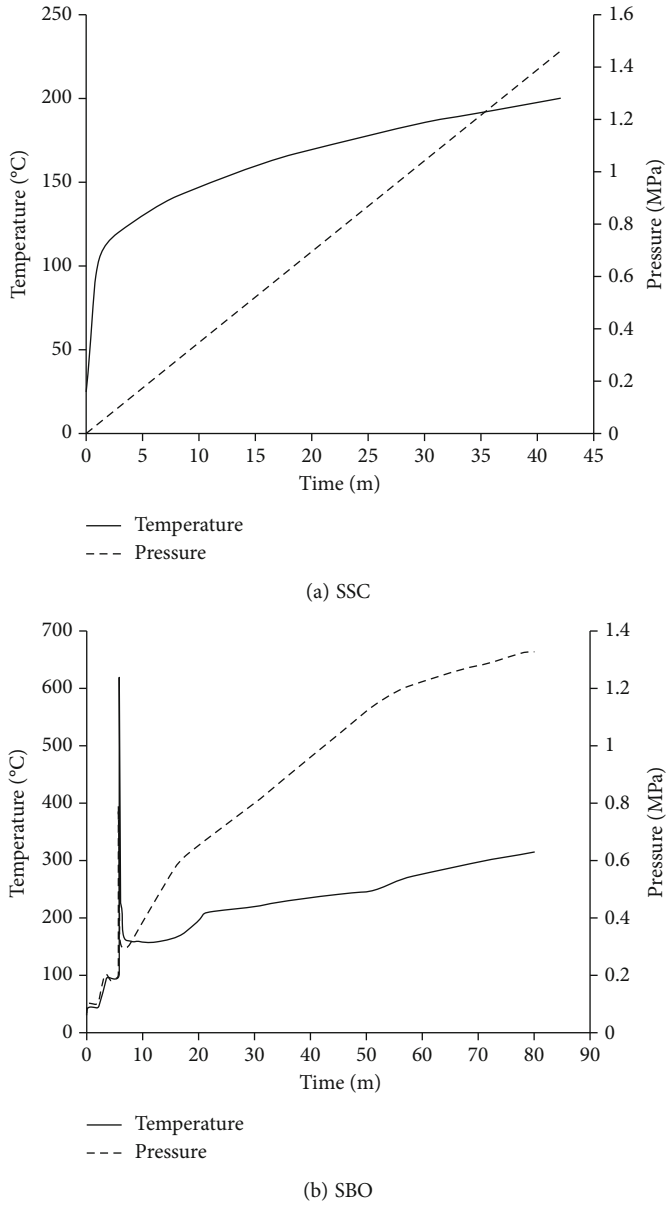

Figure 5: Pressure and temperature histories.

In the ISP48 program, concrete material properties according to temperature were selected based on an approximate "best estimate median" of the data, rather than employing bounding or conservative values [8]. The strength reduction of concrete was defined by the following equations:

$$S_{RC} = \exp^{-(T/632)^{1.8}}, \quad (1)$$

where S_{RC} represents the ratio of degraded strength to original strength, and $S_{RC} = 1$ indicates no reduction in concrete strength. However, in this study, the internal pressure capacity of a PCCV is investigated in consideration of the uncertainty in concrete material properties according to temperature instead of equation (1). To this end, the upper and lower bounds of the concrete compressive strength (f_c') presented in Figure 4(b) are applied. The reason why the consideration of the upper and lower bound instead of the probabilistic data is that sufficient research on probabilistic characteristics of concrete properties at elevated temperatures is rare at this point. Since Young's modulus (E) and tensile strength (f_{sp}) are dependent on the concrete compressive strength, the reduction rate of the parameters is determined using the existing equations as follows [34]:

$$E = 57{,}000\sqrt{f_c'}, \quad (2)$$

$$f_{sp} = 0.56 f_c'^{0.5}. \quad (3)$$

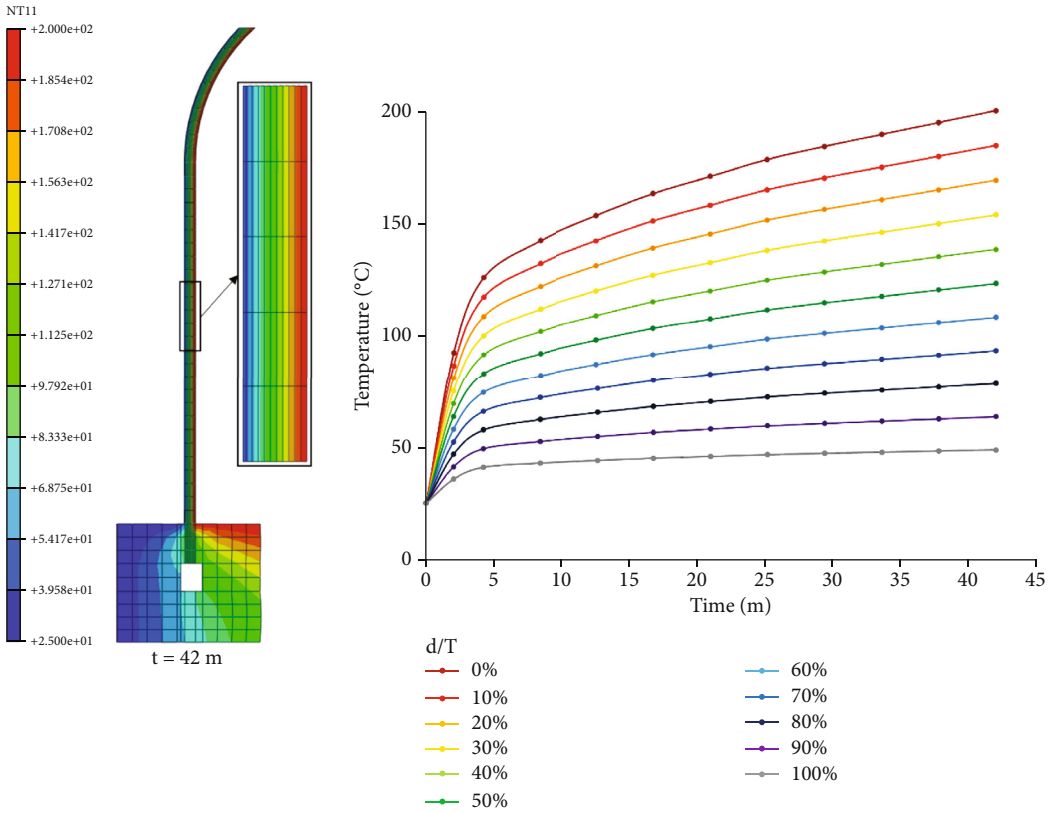

(a) Saturated steam condition: 200°C

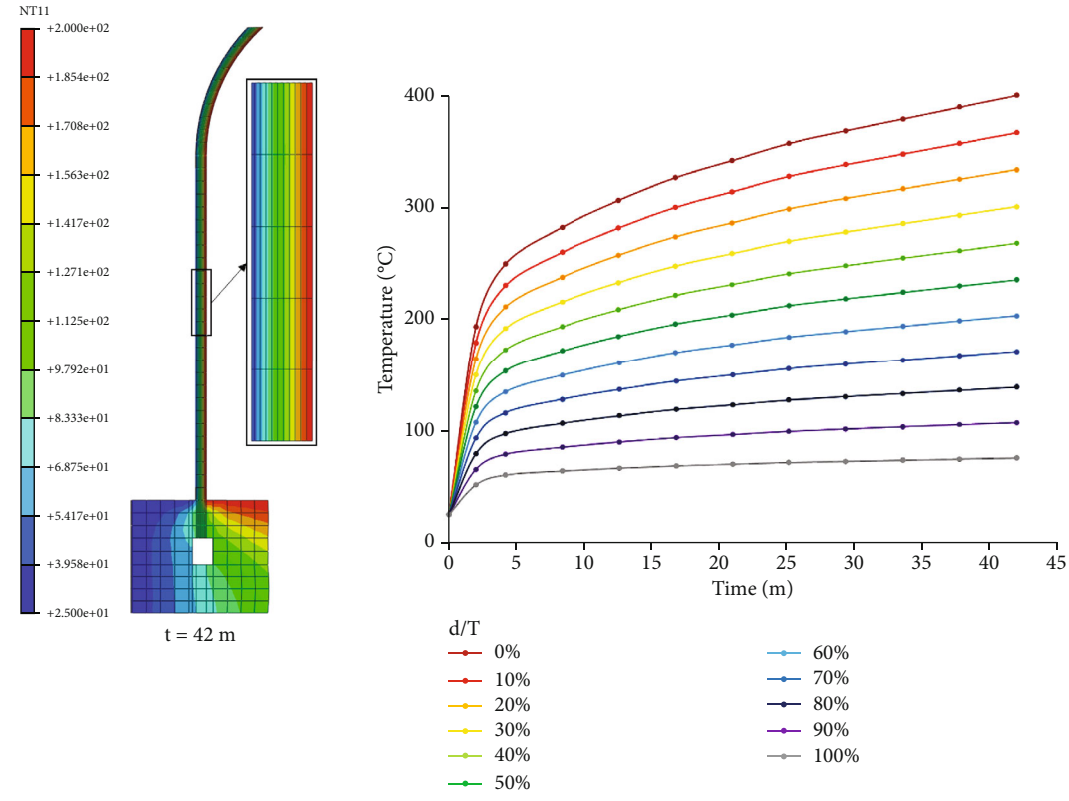

(b) Saturated steam condition: 400°C

Figure 6: Continued.

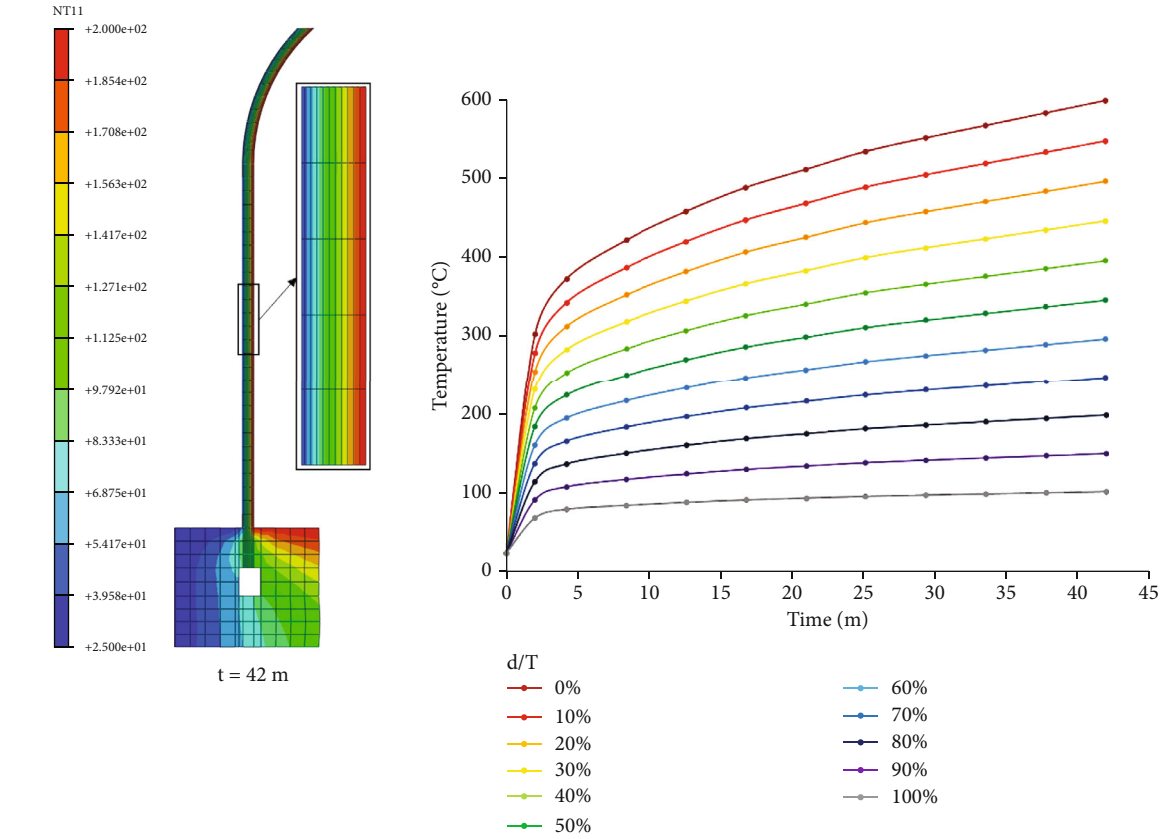

(c) Saturated steam condition: 600°C

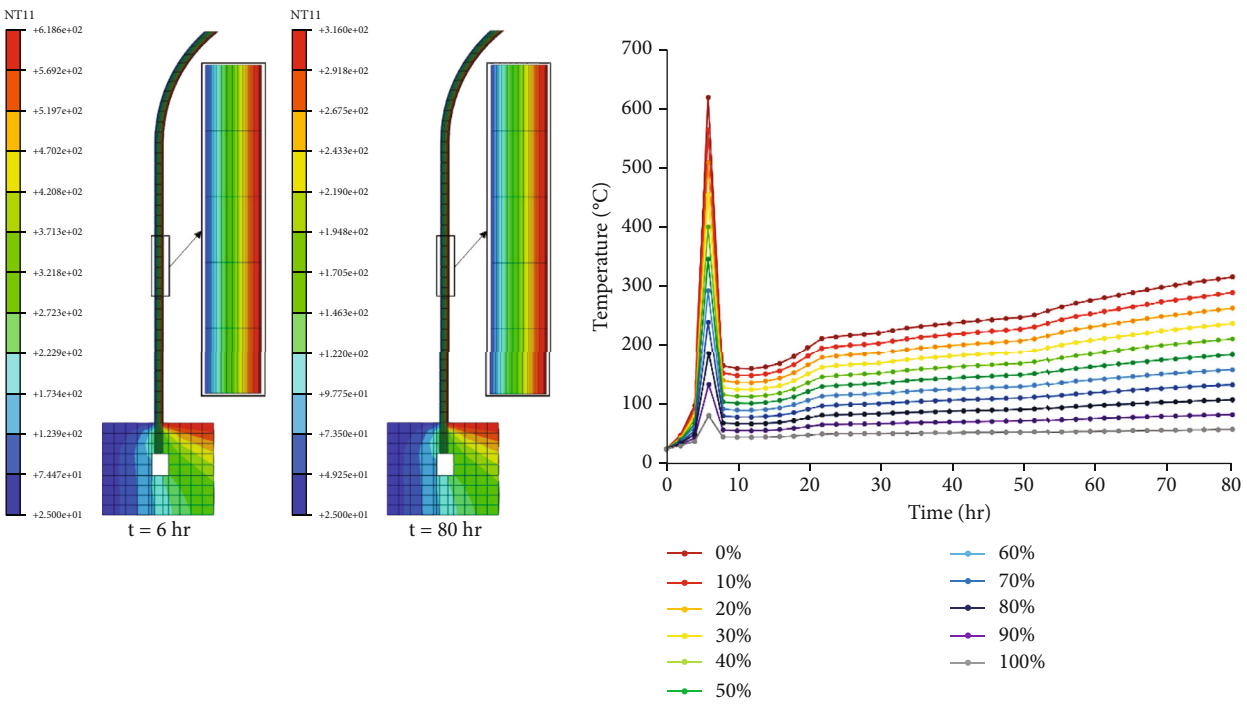

(d) Station blackout

Figure 6: Temperature distributions on concrete cylinder wall.

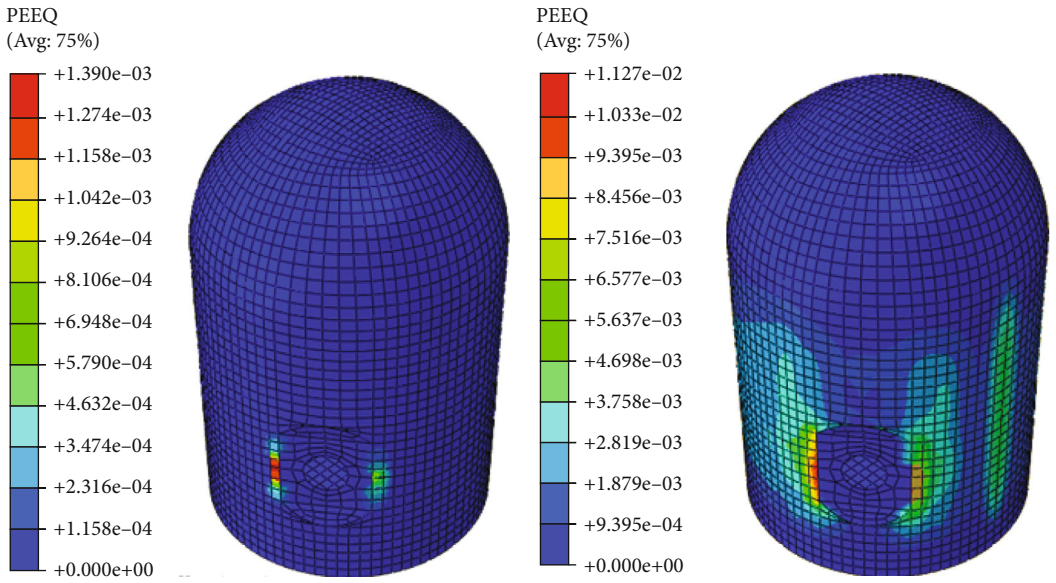

(a) Onset of leakage (2.5 P_d) (b) Functional failure (3.3 P_d)

Figure 7: Equivalent plastic strain of steel liner.

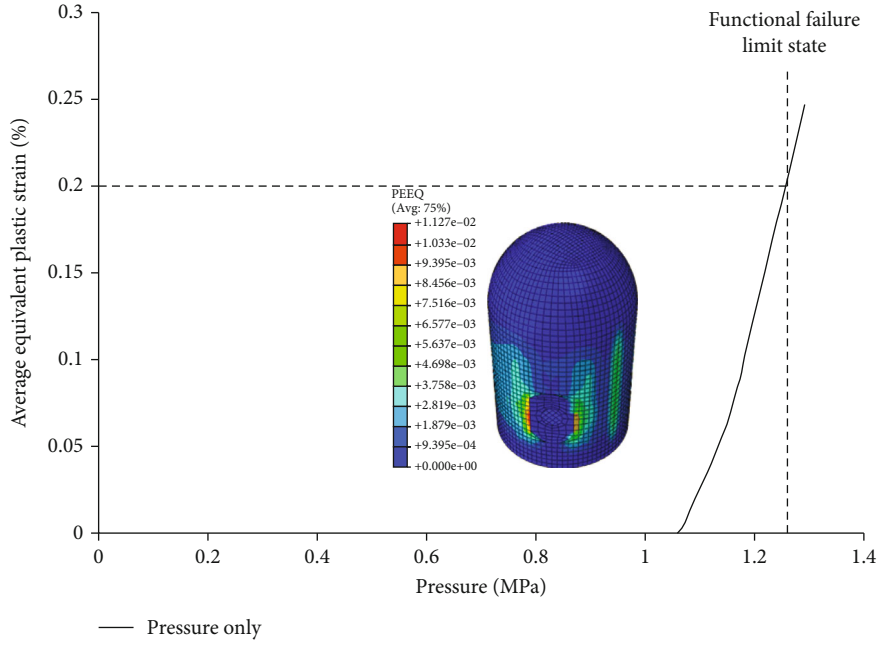

Figure 8: Average equivalent plastic strain of steel liner at global free field.

Tables 1–3 provide a summary of the residual ratios for each parameter used in this study, considering temperature variations. Regarding steel, the uncertainty in material properties is relatively insignificant compared to concrete. Therefore, the change in steel material properties with temperature is calculated deterministically using the following formula presented in the ISP program [8]:

$$S_{Rs} = \exp^{-((T-34)/300)^{1.9}}, \; T > 340 \circ C, \tag{4}$$

$$S_{Rs} = 1, \; T \leq 340 \circ C. \tag{5}$$

Here, S_{RS} represents the ratio of degraded strength to original strength for steel, with $S_{RS} = 1$ indicating no reduction in steel strength.

3.4. Heat Transfer Analysis of Containment Behavior. In this section, a comprehensive analysis of heat transfer was conducted to investigate the thermal effects on the containment behavior. Two thermal load cases recommended by International Standard Problem 48 were considered in this study.

The first load case, saturated steam conditions (SSC), represents a pseudoaccident scenario with a monotonic increase in pressure and temperature due to the saturated

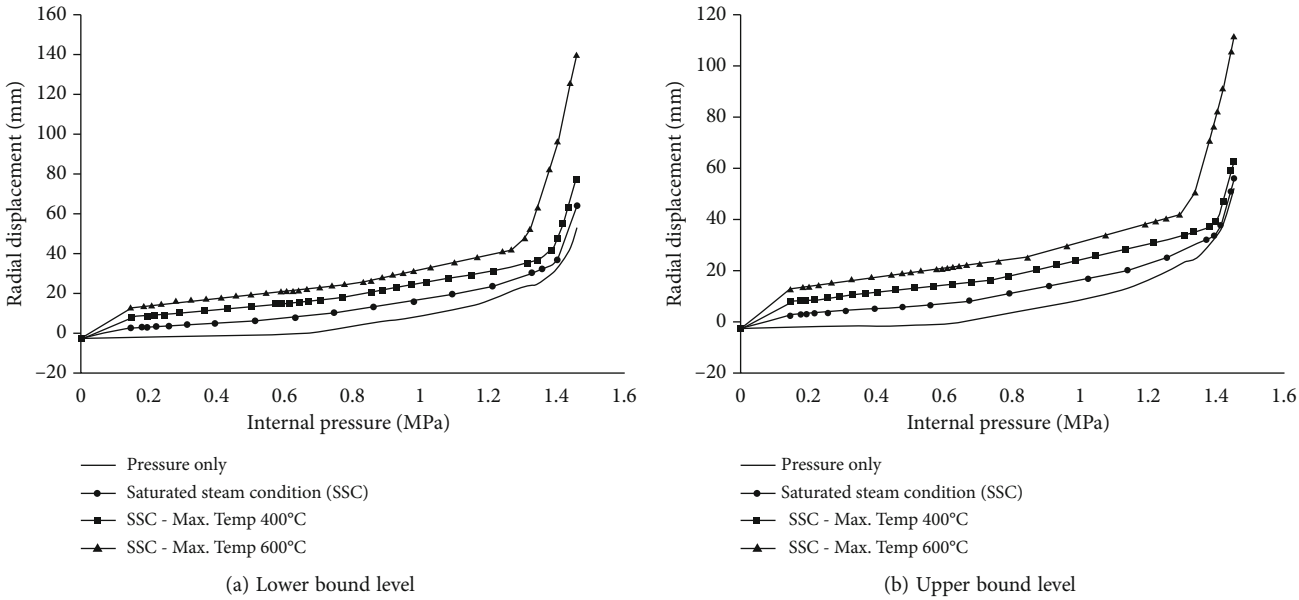

Figure 9: Radial displacement vs. internal pressure plot during SSC.

steam. Figure 5(a) illustrates the suggested temperature-pressure history, reaching up to 200°C. Additionally, scenarios with higher maximum temperatures of 400°C and 600°C were defined to assess the effects of temperature variations and changes on the containment building.

The second load case, station blackout (SBO), simulates a severe accident scenario for a four-loop PWR with a configuration and volume similar to the PCCV model. SBO is initiated by reactor coolant pump trips, followed by hydrogen burn and detonation, and dryout of the lower compartment. Figure 5(b) provides a visual representation of the SBO scenario.

Heat transfer analyses for SSC and SBO were performed by applying temperature to the liner and implementing specific boundary conditions. Convection is applied to the outer surface of concrete, including the cylinder wall and dome, while conduction is considered for the basemat. The corresponding conduction and convection coefficient are represented by the following equations:

$$\text{Conduction coefficient } h_{\text{cond}} = 4.80\ \text{W/m}^{-2} - K, \quad (6)$$

$$\text{Convection coefficient } h_{\text{conv}} = 0.0724\ \text{W/m}^{-2} - K. \quad (7)$$

Figures 6(a) and 6(d) present the temperature distributions along the thickness direction and the histories for SSC and SBO according to d/T (the depth through the thickness) ratios of 0 to 100%. Starting from an atmospheric temperature of 25°C, a smooth increase in temperature remains is observed until it approaches the maximum temperature of 200°C (and also for 400°C and 600°C SSC cases). In the case of SBO, a sudden rise and subsequent drop in temperature due to the hydrogen burn reach a peak of 618°C 6 hours after the accident, followed by a continuous increase to 316°C.

4. Case Study: Saturated Steam Condition

4.1. Limit States and Failure Criteria for Internal Pressure Capacity. In order to examine the internal pressure capacity of a containment building subjected to the combined effects of internal pressure and temperature increase, the two limit states, namely, the onset of leakage and functional failure, are defined based on experiment and analytical results.

As mentioned in the previous section, the internal pressure capacity without temperature increase was determined to be 2.5 P_d (onset of leakage state) and 3.3 P_d (functional failure state) through experiments. Correspondingly, the associated global free-field strains were recorded. However, when the temperature and internal pressure simultaneously increase, responses such as radial displacement or strain are influenced not only by internal pressure but also by temperature, making it inappropriate to rely solely on these responses for determining the internal pressure capacity. Therefore, in this study, the internal pressure capacity for each limit state under the temperature increase is determined using the equivalent plastic strain obtained through the FE analysis. Figure 7 shows the contours of the equivalent plastic strain in the liner when internal pressures of 2.5 P_d and 3.3 P_d occur without temperature increase. At the onset of the leakage limit state, the plastic deformation of the liner is concentrated in the EH region, with an equivalent plastic strain of approximately 0.14%. This value aligns with the experimental observation where leakage of the containment began at the EH part. Therefore, this value is selected as the failure criterion for calculating the internal pressure capacity at the onset of leakage under temperature increase.

The functional failure state represents the point at which the leakage of the containment is maximized. At this stage, not only the effect of the EH region but also the overall

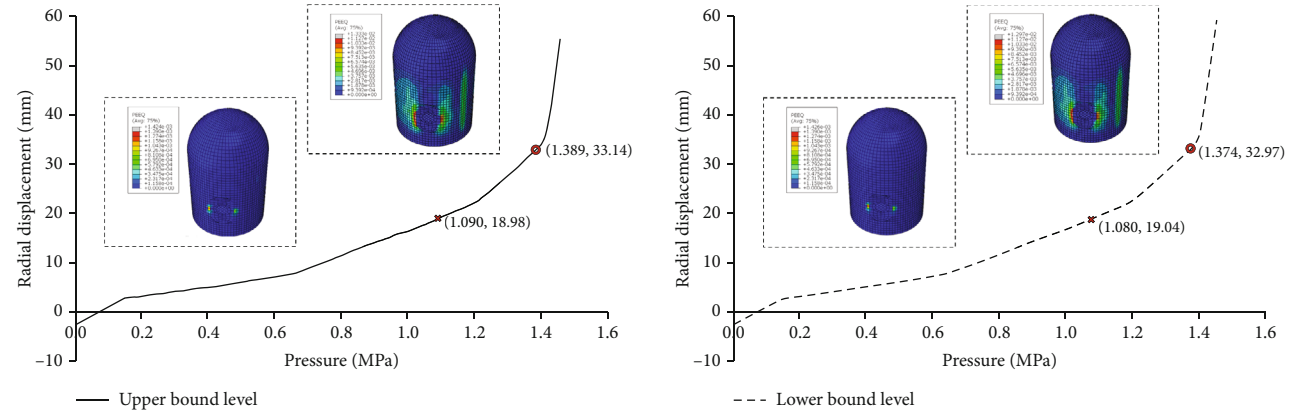

(a) 200°C case

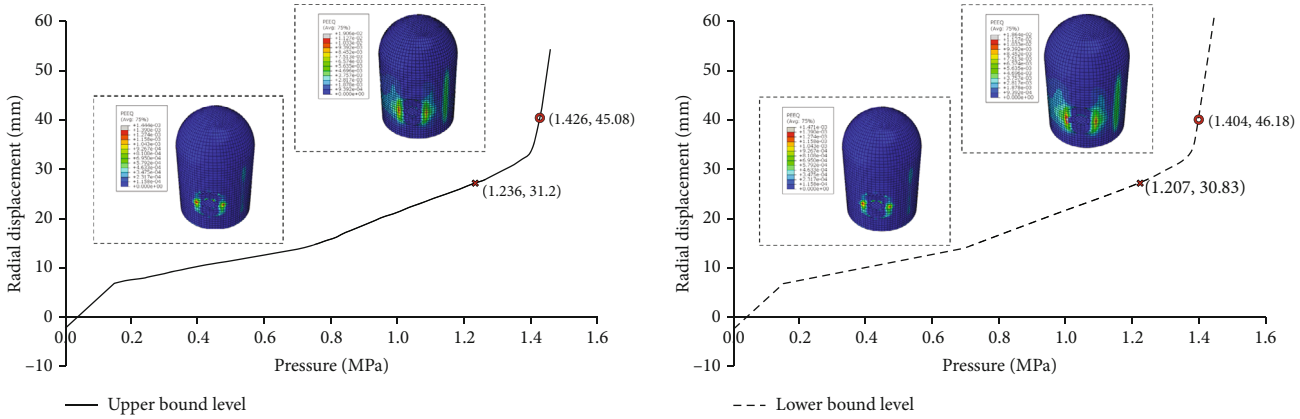

(b) 400°C case

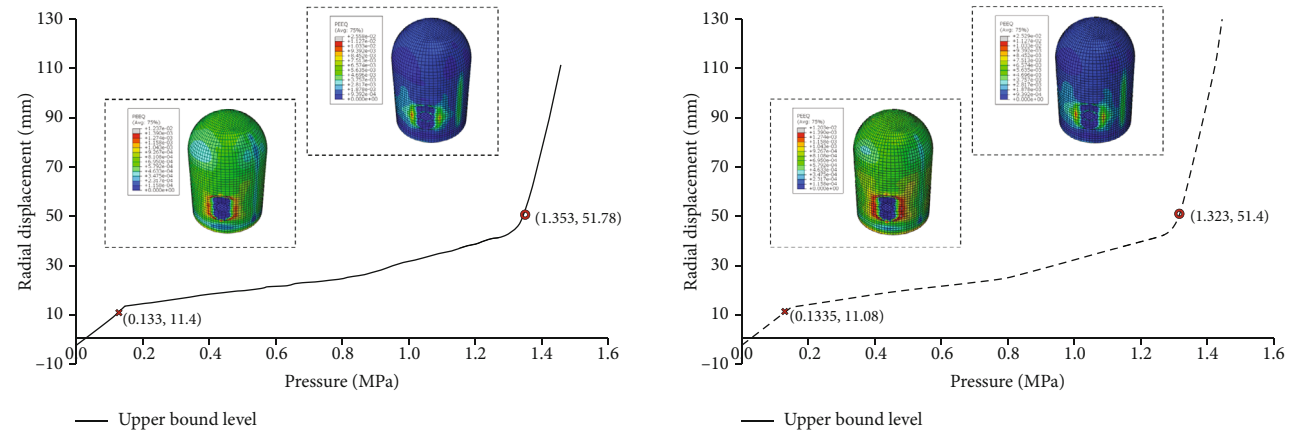

(c) 600°C case

Figure 10: Comparison of radial displacements and internal pressures.

Table 4: Variation of internal pressures due to material uncertainty under SSC (MPa).

Limit states	Uncertainty	Pressure only	200°C	400°C	600°C
Onset of leakage	Lower bound level	0.975	1.09	1.24	0.13
	Upper bound level		1.08	1.22	0.13
Functional failure	Lower bound level	1.287	1.39	1.43	1.35
	Upper bound level		1.37	1.40	1.32

behavior of the containment must be considered. Hence, the internal pressure capacity in the functional failure state is calculated using the average equivalent plastic strain in the midheight (4,260~6,200 mm) of the cylinder at an azimuth of 135 degrees. The location, known as the global free field, is chosen to ensure it is away from the influence of discontinuities or openings. As shown in Figure 8, when the internal pressure of 3.3 P_d occurred, the average equivalent plastic strain was 0.2% with a maximum plastic strain of 1.1% observed in the EH part. Therefore, an average equivalent plastic strain of 0.2% is determined as the failure criterion for the functional failure limit state.

4.2. Impact of Material Uncertainty and Temperature on Internal Pressure Capacity of PCCV. To investigate the influence of uncertainty in concrete material properties due to temperature changes on the internal pressure capacity, upper and lower boundaries of concrete compressive strength were defined in Section 3.3, while Young's modulus and tensile strength were estimated using empirical equations. The analysis of internal pressure for the containment was conducted by considering the combined effects of uncertainties and thermal analysis results. Figure 9 illustrates the variations in internal pressure and radial displacement at the global free field as a function of temperature and concrete properties. The results demonstrate a significant increase in the radial displacement of the containment with rising temperature. However, this increase is attributed not only to internal pressure but also to thermal expansion, making it insufficient to determine the extent of damage to the containment. Figure 10 and Table 4 present the internal pressure capacities based on the equivalent plastic strain for various cases, including no temperature increase and maximum temperatures of 200°C, 400°C, and 600°C. When the temperature is not considered, the pressure at the onset of the leakage limit state is 0.975 MPa, while the pressure at the functional failure limit state is 1.287 MPa. For the 200°C case, the uncertainty in concrete properties (upper and lower bound levels) due to the temperature has a negligible effect on the internal pressure capacity, resulting in internal pressure of 1.09 MPa and 1.39 MPa for the two limit states, respectively. Similarly, in the case of 400°C, the uncertainty in concrete properties does not significantly influence the internal pressure capacity, yielding pressure capacity of 1.24 MPa and 1.43 MPa. Even for the 600°C case, the effect of the uncertainty in concrete properties on the internal pressure capacity is insignificant, with estimated capacities of 0.13 MPa at the onset of the leakage limit state and 1.35 MPa at the functional failure limit state. Thus, the uncertainty in concrete material properties resulting from temperature changes does not have a substantial impact on the internal pressure capacity. This can be attributed to the temperature discrepancy between the inside and outside concrete shear walls, as revealed by the thermal analysis, leading to partial degradation rather than complete degradation of the concrete shear walls. Although a difference in material properties is up to 30% between the upper and lower levels, the overall strength reduction in the concrete shear wall is expected to be much less due to the partial degradation, so that a reduction does not significantly affect the internal pressure capacity.

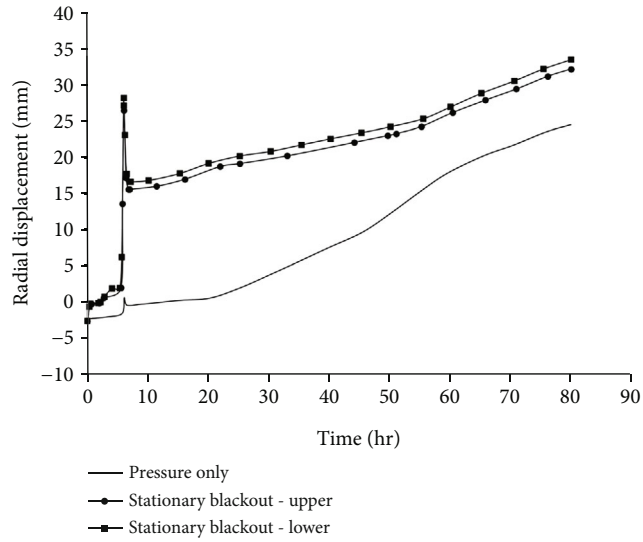

Figure 11: Radial displacement vs. internal pressure plot during SBO.

However, the effect of temperature on the internal pressure capacity is apparent. The pressure capacity increases with rising temperature in all cases except for the 600°C scenario at the onset of the leakage limit state. This indicates a delay in the internal pressure capacity as the temperature increases. The containment building experiences thermal expansion during temperature rise, but the thermal analysis reveals different temperature distributions within the concrete shear wall depending on its thickness. The discrepancy results in the suppression of thermal expansion of the steel liner. In other words, while the interior tends to expand, the unaffected exterior tries to restrict this expansion. As a result, an additional compressive stress is induced on the liner, similar to concrete beams subjected to prestressing, which positively affects the pressure capacity and ultimately increases its resistance. On the other hand, in the 600°C case, the temperature reaches 340°C and exceeds 400°C at the beginning of the analysis, as shown in Figure 6(c), initiating a 5% reduction in steel strength. Consequently, yielding near the EH occurs, leading to leakage despite very low internal pressure. Thus, this effect is attributed to the degradation of the steel strength rather than the effect of pressure, causing early onset of leakage due to local yield of the liner. The reduction in steel strength also affects the pressure capacity at the functional failure limit state, resulting in smaller pressure values compared to the 200°C and 400°C cases. Nevertheless, the delay effect of the internal pressure capacity persists even at high temperatures when compared to the scenario without any temperature increase.

5. Analysis of Containment Behavior in a Station Blackout Scenario

This section focuses on the impact of the temperature-induced uncertainty in material properties on the behavior of the containment structure, specifically in the context of a station blackout (SBO) scenario for a pressurized water reactor with a configuration and volume similar to the PCCV model. The

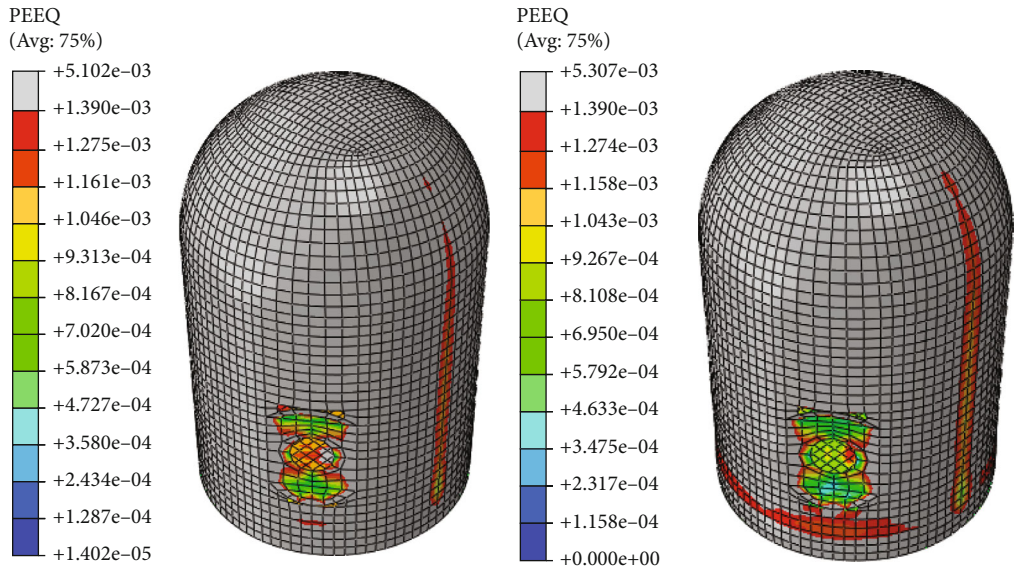

(a) Lower bound level (0.1095 MPa) (b) Upper bound level (0.11 MPa)

Figure 12: Equivalent plastic strain of steel liner at onset of leakage limit state.

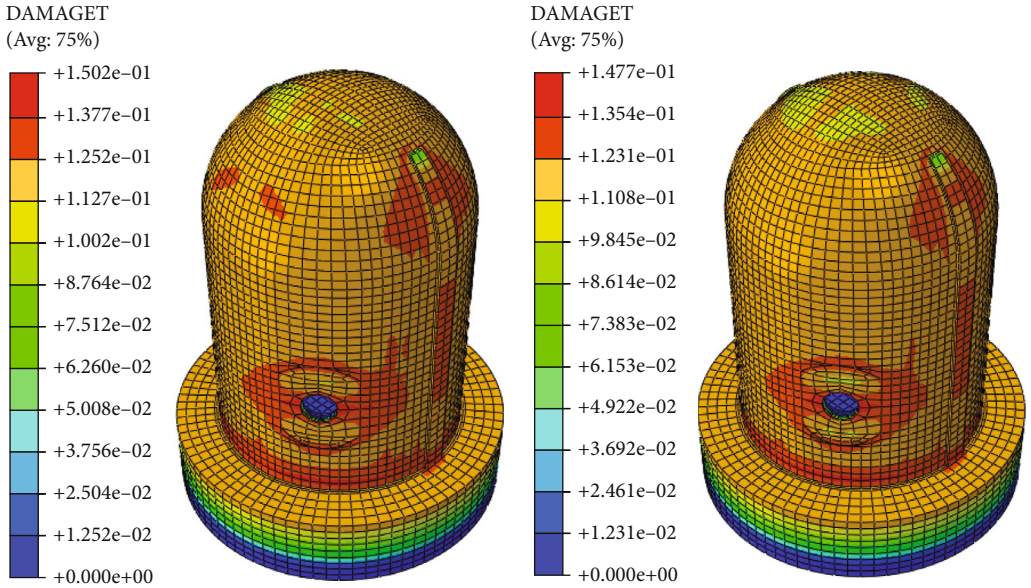

(a) Lower bound level (0.1095 MPa) (b) Upper bound level (0.11 MPa)

Figure 13: Damage of cylinder concrete wall at onset of leakage limit state.

SBO involves a rapid temperature increase of up to 600°C due to hydrogen burn, as depicted in Figure 5(b). A comprehensive analysis of severe accident progression during SBO was performed using the MELCOR code [8, 35].

Figures 11–15 and Table 5 present the results considering the uncertainty of material properties for temperature changes. Figure 11 shows that the radial displacement of the upper level is slightly smaller than that of the lower level, although the difference is not significant. Therefore, the uncertainty in the material properties due to the temperature change does not significantly alter the overall behavior of the containment structure. Figures 12 and 13 compare the equivalent plastic strain of the steel liner and the damage to the concrete shear wall at the onset of the leakage. The analysis reveals that the variation in internal pressure capacity resulting from uncertainty in material properties was inconsiderable, as both the steel liner and concrete shear walls exhibit similar behaviors irrespective of the uncertainty. Similarly, Figures 14 and 15 compare the equivalent plastic strain of the steel liner and the damage to the concrete shear wall at the functional failure limit state. The findings indicate no significant change in the internal pressure capacity, and both steel liner and concrete shear walls display consistent results regardless of the uncertainty.

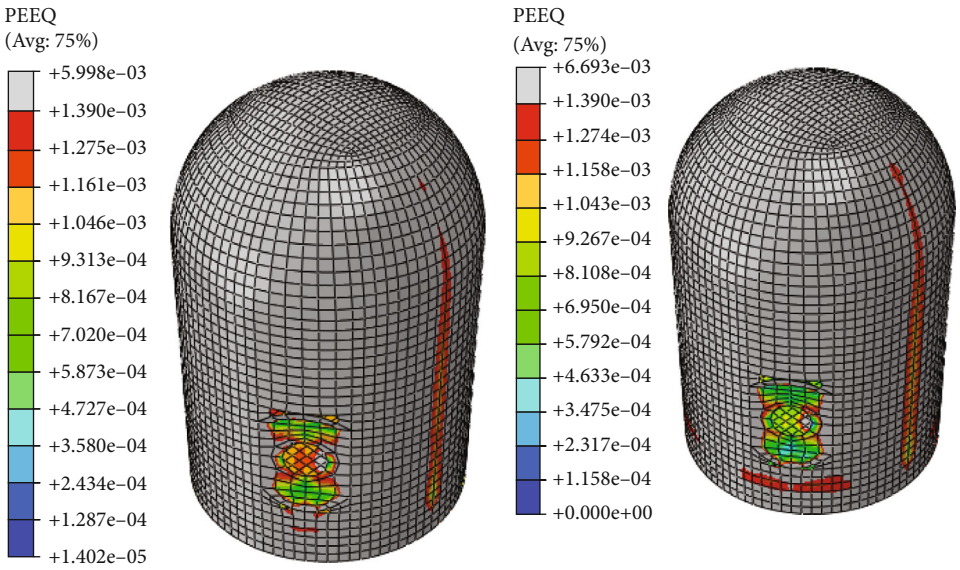

(a) Lower bound level (0.117 MPa) (b) Upper bound level (0.120 MPa)

Figure 14: Equivalent plastic strain of steel liner at functional failure limit state.

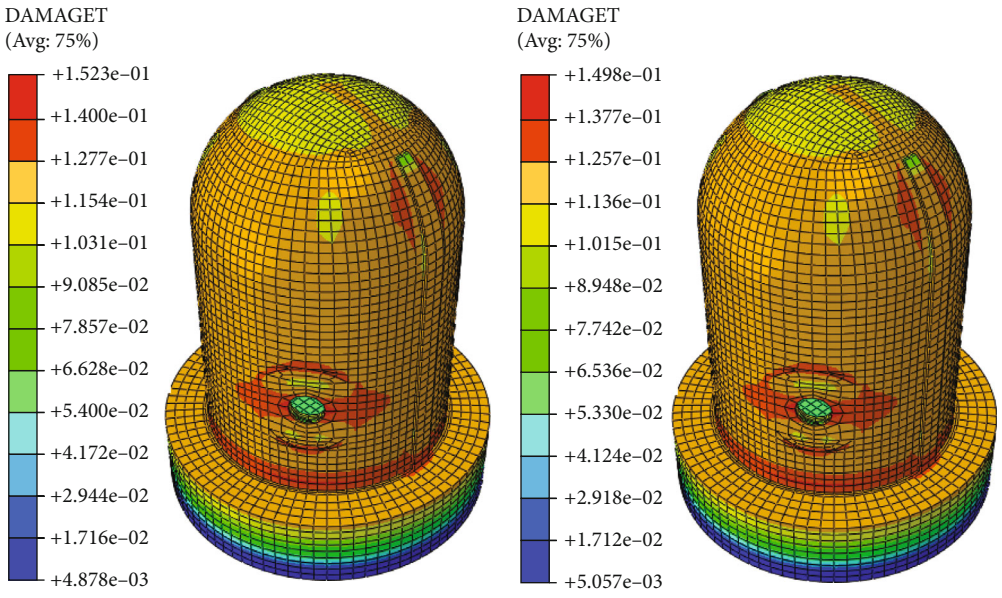

(a) Lower bound level (0.117 MPa) (b) Upper bound level (0.120 MPa)

Figure 15: Damage of cylinder concrete wall at functional failure limit state.

The internal pressure capacity at the onset of leakage and functional failure limit state is approximately 0.11 MPa and 0.12 MPa, respectively, suggesting that the onset of leakage and functional failure occur almost simultaneously during the SBO scenario. As illustrated in Figure 12, unlike the case without temperature effects, both the EH part and a significant portion of the liners exceed the yield strain at the onset of the leakage state. It indicates that liner deformation or tearing can occur solely due to the expansion of the liner caused by the rapid elevation of temperature. Furthermore, at the functional failure limit state, the average equivalent plastic strain at the global free field exceeds 0.2% during the rapid temperature change, despite the relatively low internal pressure. Thus, it is evident that the effect of temperature is considerably more pronounced than the effect of internal pressure.

Table 5: Variation of internal pressures due to material uncertainty under SBO (MPa).

Limit states	Uncertainty	Pressure only	SBO
Onset of leakage	Lower level	0.975	0.1095
	Upper level		0.110
Functional failure	Lower level	1.287	0.117
	Upper level		0.120

6. Conclusions

The effect of internal pressure combined with various temperature changes on the internal pressure capacity of the PCCV in terms of leakage is evaluated in this study. Moreover, the influence of uncertainty in concrete material properties resulting from the temperature changes on the internal pressure capacity is identified. The conclusion of this study can be summarized as follows:

(i) The uncertainty in concrete material due to SSC scenarios was revealed to have little influence on the internal pressure capacity of the containment vessel. This lack of impact is because of the temperature difference between the interior and exterior concrete shear walls, as indicated by thermal analysis. This temperature discrepancy leads to only partial degradation of the inner shear walls, rather than complete degradation across the entire thickness. Consequently, the overall strength reduction of the concrete shear walls is expected to be insignificant

(ii) The SSC analysis clearly demonstrates the variation in internal pressure capacity with temperature changes, showing an increasing trend as the temperature rises. This behavior is attributed to the restraining effect of the exterior concrete walls on the expansion of the steel liner caused by temperature increase. The temperature difference between the inside and outside of the thick concrete walls generates additional compressive stress on the liner, resulting in a delayed response of the internal pressure capacity under temperature conditions

(iii) In the case of an SSC assuming up to 600°C, the internal temperature exceeds 340°C very early, and the steel liner begins to degrade. Consequently, the yielding of the liner due to the temperature change occurs exclusively at the EH region despite the very low internal pressure. Therefore, the onset of leakage is closely related to how quickly the temperature (around 340~400°C), which can reduce the strength of the liner, can be exceeded rather than the increase in the internal pressure

(iv) Regarding the SBO scenario involving a rapid temperature change of up to 600°C due to the hydrogen burn, the impact of uncertainty in concrete material properties resulting from temperature changes on the internal pressure capacity of the containment building is found to be insignificant, similar to the SSC case. However, the analyses indicate that such high levels of rapid temperature change (hydrogen burn) are expected to lead to almost simultaneous occurrences of leakage and functional failure

This study clearly presents the internal pressure capacity of PCCV subjected to internal pressure, and elevated temperature could increase the internal pressure capacity when plastic strain is considered as a limit state. However, in practice, the conservative value of global hoop strain, which simultaneously includes thermal and structural effects, is still used for the limit state for the design and safety evaluation of PCCV. Thus, additional experimental and analytical research on the PCCV subjected to internal pressure and elevated temperature for various cases is required to consider the use of plastic strain for the PCCV subjected to internal pressure and elevated temperature as a further study.

Data Availability

Data available on request.

Conflicts of Interest

The authors declare that they have no conflicts of interest.

Authors' Contributions

Sangwoo Lee and Woo-Min Cho are co-first authors in this paper.

Acknowledgments

This work was supported by the Nuclear Safety Research Program through the Korea Foundation of Nuclear Safety (KoFONS) using the financial resource granted by the Nuclear Safety and Security Commission (NSSC) of the Republic of Korea (No. 2106034).

References

[1] J. Yan, Y. Lin, Z. Wang, T. Fang, and J. Ma, "Failure mechanism of a prestressed concrete containment vessel in nuclear power plant subjected to accident internal pressure," *Annals of Nuclear Energy*, vol. 133, pp. 610–622, 2019.

[2] B. De Boeck, "A review of containment accidents," *Nuclear Engineering and Design*, vol. 145, no. 3, pp. 279–288, 1993.

[3] S. H. Rizkalla, S. H. Simmonds, and J. G. MacGregor, "Prestressed concrete containment model," *Journal of Structural Engineering*, vol. 110, no. 4, pp. 730–743, 1984.

[4] D. Twidale and R. Crowder, "Sizewell 'B'-a one tenth scale containment model test for the UK PWR programme," *Nuclear Engineering and Design*, vol. 125, no. 1, pp. 85–93, 1991.

[5] R. M. Parmar, T. Singh, I. Thangamani, N. Trivedi, and R. K. Singh, "Over-pressure test on BARCOM pre-stressed concrete containment," *Nuclear Engineering and Design*, vol. 269, pp. 177–183, 2014.

[6] D. S. Horschel and J. Jung, "Construction and analysis of a 1/6th-scale concrete containment model," in *Proceedings of the Third Workshop on Containment Integrity, NUREG/CR-0076, SAND86-0618*, pp. 407–428, Sandia National Laboratories, 1986.

[7] M. F. Hessheimer, E. W. Klamerus, L. D. Lamber, G. S. Rightley, and R. A. Dameron, *Overpressurization Test of a 1: 4 Scale Prestressed Concrete Containment Vessel Model*, Technical Report No. NUREG/CR-6810, SAND2003-0840P, U.S, Nuclear Regulatory Commission, Washington, DC, USA, 2003.

[8] M. F. Hessheimer and E. Mathet, "International standard problem no. 48," in *Containment Capacity, NEA/CSNI/R (2005)5*, OECD Nuclear Energy Agency, Paris, FR, 2005.

[9] H. W. Song, S. H. Nam, B. Shim, and S. H. Kim, "Path-dependent nonlinear analysis of a concrete reactor containment vessel subjected to internal pressure using a volume control technique," *Engineering Structures*, vol. 31, no. 4, pp. 990–998, 2009.

[10] S. Jiménez, A. Cornejo, L. G. Barbu, A. H. Barbat, and S. Oller, "Failure pressure analysis of a nuclear reactor prestressed concrete containment building," *Engineering Structures*, vol. 236, article 112052, 2021.

[11] S. H. Noh, I. H. Moon, J. B. Lee, and J. H. Kim, "Analysis of prestressed concrete containment vessel (PCCV) under severe accident loading," *Nuclear Engineering and Technology*, vol. 40, no. 1, pp. 77–86, 2008.

[12] A. Shokoohfar and A. Rahai, "Nonlinear analysis of prestressed concrete containment vessel (PCCV) using the damage plasticity model," *Nuclear Engineering and Design*, vol. 298, pp. 41–50, 2016.

[13] C. Zhang, P. Chen, J. Zhang et al., "Evaluation of the structural integrity of the CPR1000 PWR containment under steam explosion accidents," *Nuclear Engineering and Design*, vol. 278, pp. 632–643, 2014.

[14] T. Meng, L. Jason, T. Heits, and B. Richard, "Numerical methodology on prestressed reinforced concrete containment building: Creep, aging and leakage. Application to VERCORS mock-up," *Engineering Structures*, vol. 280, article 115625, 2023.

[15] G. N. Freskakis, R. C. Burrow, and E. B. Debbas, "Strength properties of concrete at elevated temperatures," in *Civil Engineering Nuclear Power, 1*, ASCE National Convention, Boston, 1979.

[16] V. Kodur, "Properties of Concrete at Elevated Temperatures," *International Scholarly Research Notices*, vol. 2014, Article ID 468510, 15 pages, 2014.

[17] W. M. Cho, S. K. Ha, S. Kang, and Y. S. Chang, "A numerical approach for assessing internal pressure capacity at liner failure in the expanded free-field of the prestressed concrete containment vessel," *Nuclear Engineering and Technology*, vol. 55, no. 10, pp. 3677–3691, 2023.

[18] J. Lubliner, J. Oliver, S. Oller, and E. Oñate, "A plastic-damage model for concrete," *International Journal of Solids and Structures*, vol. 25, no. 3, pp. 299–326, 1989.

[19] J. Lee and G. L. Fenves, "Plastic-damage model for cyclic loading of concrete structures," *Journal of Engineering Mechanics*, vol. 124, no. 8, pp. 892–900, 1998.

[20] G. A. Khoury, "Compressive strength of concrete at high temperatures: a reassessment," *Magazine of Concrete Research*, vol. 44, no. 161, pp. 291–309, 1992.

[21] M. S. Abrams, "Compressive strength of concrete at temperatures to 1600F," *ACI Symposium Publication*, vol. 25, pp. 33–58, 1971.

[22] M. Klisinski, "Degradation and plastic deformation of concrete," *Polish Academy of Sciences, Iftr Report*, vol. 38, 1985.

[23] M. Holmes, R. D. Anchor, M. D. Cook, and R. N. Crook, "The effects of elevated temperatures on the strength properties of reinforcing and prestressing steels," *The Structural Engineer*, vol. 60B, no. 1, 1982.

[24] P. Code, *Eurocode 3: Design of Steel Structures-Part 1-2: General Rules-Structural Fire Design*, European Committee for Standardization, London, 2007.

[25] Z. P. Bazant and M. F. Kaplan, *Concrete at High Temperatures – Material Properties and Mathematical Models*, Concrete Design and Construction Series, Longman Group Limited, 1996.

[26] O. Arioz, "Effects of elevated temperatures on properties of concrete," *Fire Safety Journal*, vol. 42, no. 8, pp. 516–522, 2007.

[27] DeFish-Price, C (Rockwell International Report), *Effects of long-term exposure to elevated temperatures on the mechanical properties of Hanford Concrete*, A construction technology laboratories report for the U.S. Department of Energy under Contract DE-AC06-77RL01030, 1981.

[28] Y. F. Chang, Y. H. Chen, M. S. Sheu, and G. C. Yao, "Residual stress-strain relationship for concrete after exposure to high temperatures," *Cement and Concrete Research*, vol. 36, no. 10, pp. 1999–2005, 2006.

[29] EN 1992-1-2-2004, *Eurocode 2- design of concrete structures part 1-2 general rules-structural fire design*, European Committee for Standardization (CEN), Brussels, 2004.

[30] T. T. Lie, T. J. Rowe, and T. D. Lin, "Residual strength of fire exposed RC columns evaluation and repair of fire damage to concrete," *American Concrete Institute*, vol. 92, pp. 153–174, 1986.

[31] Z. P. Bazant and J. C. Chern, "Stress-induced thermal and shrinkage strains in concrete," *Journal of Engineering Mechanics*, vol. 113, no. 10, pp. 1493–1511, 1987.

[32] M. J. Terro, "Numerical modeling of the behavior of concrete structures in fire," *ACI Structural Journal*, vol. 95, no. 2, 1998.

[33] D. A. Krishna, R. S. Priyadarsini, and S. Narayanan, "Effect of elevated temperatures on the mechanical properties of concrete," *Procedia Structural Integrity*, vol. 14, pp. 384–394, 2019.

[34] ACI Committee 318-95, *Building code requirements for structural concrete (ACI 318-95) and commentary (ACI 318R-95)*, An ACI Standard, American Concrete Institute, Farmington Hills, Michigan 48333-9094, 1995.

[35] MELCOR Computer Code Manuals, *NUREG/Cr-6119, SAND2000-2417*, Sandia National Laboratories, Albuquerque, NM, 2000.